Article

Stepwise Hydration of Ionized Aromatics. Energies, Structures of the Hydrated Benzene Cation, and the Mechanism of Deprotonation Reactions

Yehia M. Ibrahim, Michael Meot-Ner, Edreese H. Alshraeh, M. Samy El-Shall, and Steve Scheiner

J. Am. Chem. Soc., **2005**, 127 (19), 7053-7064• DOI: 10.1021/ja050477g • Publication Date (Web): 26 April 2005

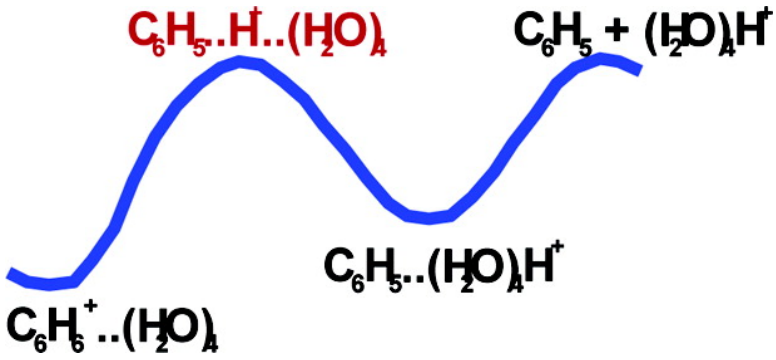

More About This Article

Additional resources and features associated with this article are available within the HTML version:

- Supporting Information
- Links to the 6 articles that cite this article, as of the time of this article download
- Access to high resolution figures
- Links to articles and content related to this article
- Copyright permission to reproduce figures and/or text from this article

View the Full Text HTML

J|A|C|S
ARTICLES
Published on Web 04/26/2005

Stepwise Hydration of Ionized Aromatics. Energies, Structures of the Hydrated Benzene Cation, and the Mechanism of Deprotonation Reactions

Yehia M. Ibrahim,[†,§] Michael Meot-Ner (Mautner),[†] Edreese H. Alshraeh,[†] M. Samy El-Shall,*[,†] and Steve Scheiner[‡]

Contribution from the Department of Chemistry, Virginia Commonwealth University, Richmond, Virginia 23284, and Department of Chemistry, Utah State University, Logan, Utah 84322

Received January 24, 2005; E-mail: selshall@hsc.vcu.edu

Abstract: The stepwise binding energies ($\Delta H°_{n-1,n}$) of 1−8 water molecules to benzene$^{\bullet+}$ [$Bz^{\bullet+}(H_2O)_n$] were determined by equilibrium measurements using an ion mobility cell. The stepwise hydration energies, $\Delta H°_{n-1,n}$, are nearly constant at 8.5 ± 1 kcal mol^{-1} from $n = 1-6$. Calculations show that in the $n = 1-4$ clusters, the benzene$^{\bullet+}$ ion retains over 90% of the charge, and it is externally solvated, that is, hydrogen bonded to an $(H_2O)_n$ cluster. The binding energies and entropies are larger in the $n = 7$ and 8 clusters, suggesting cyclic or cage-like water structures. The concentration of the $n = 3$ cluster is always small, suggesting that deprotonation depletes this ion, consistent with the thermochemistry since associative deprotonation $Bz^{\bullet+}(H_2O)_{n-1} + H_2O \rightarrow C_6H_5^{\bullet} + (H_2O)_nH^+$ is thermoneutral or exothermic for $n \geq 4$. Associative intracluster proton transfer $Bz^{\bullet+}(H_2O)_{n-1} + H_2O \rightarrow C_6H_5^{\bullet}(H_2O)_nH^+$ would be also exothermic for $n \geq 4$, but lack of H/D exchange with D_2O shows that the proton remains on $C_6H_6^{\bullet+}$ in the observed $Bz^{\bullet+}(H_2O)_n$ clusters. This suggests a barrier to intracluster proton transfer, and as a result, the $[Bz^{\bullet+}(H_2O)_n]^*$ activated complexes either undergo dissociative proton transfer, resulting in deprotonation and generation of $(H_2O)_nH^+$, or become stabilized. The rate constant for the deprotonation reaction shows a uniquely large negative temperature coefficient of $k = cT^{-67\pm4}$ (or activation energy of −34 ± 1 kcal mol^{-1}), caused by a multibody mechanism in which five or more components need to be assembled for the reaction.

I. Introduction

The interactions between aromatic hydrocarbons and water play important roles in many chemical, biological, and physical processes, such as the conformation and folding of proteins, base pair stacking in DNA, drug design, macromolecular assemblies, biological membranes, clathrate hydrate formation, micelles, and several other examples.[1−7] Hydrogen bonding interactions involving ionized aromatics are important in radiation chemistry, electrochemistry, and polymerization in aqueous solvents and in astrochemical environments.[8−10] Specifically, extraction of protons from ionized aromatics by solvent molecules may have important implications for reaction mechanisms, inhibition, and termination of polymerization, and for astrochemical processes.[11−14] For example, the crucial role played by the presence of trace amounts of water and other protonic impurities on the mechanism and rate of cationic polymerization of aromatic monomers, such as styrene, is widely recognized.[9] The ionic mechanism usually prevails only in very dry systems, while radical polymerization dominates in the presence of water.[9] These interactions and processes are not well characterized at the molecular level, and much of our understanding is based on chemical intuition and approximate theoretical descriptions.[4,5] Insight into the basic molecular interactions would be obtained from the energies and structures of the key species involved in the gas phase stepwise hydration of a typical aromatic molecule, such as benzene, or a radical cation, such as $C_6H_6^{\bullet+}$. Therefore, the $(C_6H_6)(H_2O)_n$ and $(C_6H_6^{\bullet+})(H_2O)_n$ cluster systems can be considered as prototypical models for understanding the molecular aspects leading to *hydrophobic hydration* in macroscopic systems.

† Virginia Commonwealth University.
‡ Utah State University.
§ Current address: Pacific Northwest National Laboratory, Richland, WA.

(1) Ball, P. *H_2O: A Biography of Water*; Weidenfeld & Nicolson: London, 1999.
(2) Jeffrey, G. A.; Saenger, W. *Hydrogen Bonding in Biological Structures*; Springer-Verlag: Berlin, New York, 1991.
(3) Jeffrey, G. A. *An Introduction to Hydrogen Bonding*; Oxford University Press: Oxford, 1997.
(4) Ben-Naim, A. *Hydrophobic Interactions*; Plenum: New York, 1980.
(5) Israelachvili, J. N. *Intermolecular and Surface Forces*, 2nd ed.; Academic Press: San Diego, CA, 1992.
(6) Tanford, C. *The Hydrophobic Effect: Formation of Micelles and Biological Membranes*, 2d ed.; Wiley: New York, 1980.
(7) Sloan, E. D. *Clathrate Hydrates of Natural Gases*; M. Dekker: New York, 1990.
(8) Conway, B. E. *Ionic Hydration in Chemistry and Biophysics*; Elsevier: Amsterdam, New York, 1981.
(9) Kennedy, J. P.; Marechal, E. *Carbocationic Polymerization*; John Wiley & Sons: New York, 1982.
(10) Woon, D. E.; Park, J.-Y. *Astrophys. J.* **2004**, *607*, 342−345.
(11) Daly, G. M.; Meot-Ner, M.; Pithawalla, Y. B.; El-Shall, M. S. *J. Chem. Phys.* **1996**, *104*, 7965−7973.
(12) Workentin, M. S.; Johnston, L. J.; Wayner, D. D. M.; Parker, V. D. *J. Am. Chem. Soc.* **1994**, *116*, 8279−8287.
(13) Silverman, J.; Tagawa, S.; Kobayashi, H.; Katsumura, Y.; Washio, M.; Tabata, Y. *Radiat. Phys. Chem.* **1983**, *22*, 1039−1042.
(14) Gudipati, M. S.; Allamandola, L. J. *Astrophys. J.* **2003**, *596*, L195−L198.

The structure, spectroscopy, and solvation of $(C_6H_6)(H_2O)_n$ clusters have been a subject of extensive experimental and theoretical studies and continue to attract much attention.[15−18] These studies have established several characteristic features for the interaction of the π-system with multiple water molecules. Among these features are the tendency of the water molecules to form a hydrogen bonding subcluster above the benzene ring with weak π-hydrogen connecting the water and the benzene moieties and the very efficient fragmentation of the photoionized clusters, which has been interpreted as a direct consequence of the hydrogen bonding to the benzene ring.[15] Upon ionization, the positive charge on the aromatic ring repels the hydrogen atoms of water, thus resulting in a significant structural change which leads to very efficient fragmentation. Therefore, the structures of the neutral $(C_6H_6)(H_2O)_n$ clusters are very different from the $(C_6H_6^{\bullet+})(H_2O)_n$ cluster cations.

Unlike the extensive studies of the neutral benzene−water clusters, only a few studies have been reported on the $(C_6H_6^{\bullet+})(H_2O)_n$ cluster cations.[19−26] These studies involve mass spectrometric investigation of photoionized benzene(water)$_n$ clusters[19] and IR[20−25] and electronic[26] spectroscopy of the cations generated by the collision of bare benzene cations with water clusters[22] or with water molecules followed by a supersonic adiabatic expansion.[25] The mass spectrometric study of the photoionized neutral clusters provided indirect evidence for the intracluster proton transfer reaction within large $(C_6H_6^{\bullet+})(H_2O)_n$ cluster cations with $n > 20$ through the observation of magic numbers similar to those typically observed in large $H^+(H_2O)_n$ clusters.[19,27] The IR spectra of the $(C_6H_6^{\bullet+})(H_2O)_n$ cluster cations exhibit a drastic change between the $n = 3$ and $n = 4$ clusters, where only aromatic CH stretching bands appear in the spectra of the $n \leq 3$ cations, while broadened absorptions assigned to hydrogen-bonded OH stretches appear in the spectra of $n \geq 4$ clusters.[20−23] The IR spectra for larger cluster cations ($n = 4-23$) show features almost identical to those of protonated water clusters $H^+(H_2O)_n$,[28,29] thus providing strong evidence for the intracluster proton transfer reaction from the $C_6H_6^{\bullet+}$ to the water subcluster.[25] Electronic spectroscopy of the $(C_6H_6^{\bullet+})(H_2O)_n$ clusters also provides further evidence for the occurrence of the intracluster proton transfer reaction at $n = 4$.[26]

Despite compelling evidence from the spectroscopic studies of the $(C_6H_6^{\bullet+})(H_2O)_n$ cluster cations for the proton transfer reaction at $n \geq 4$,[20−26] the mechanism of the reaction and its temperature dependence are not clearly characterized. For example, the IR photodissociation studies of the $(C_6H_6^{\bullet+})(H_2O)_n$ cations showed that the $(C_6H_6^{\bullet+})(H_2O)_{n-1}$ or $(C_6H_5^{\bullet})H^+(H_2O)_{n-1}$ fragment was the unique fragment upon IR excitation, but only the $C_6H_6^{\bullet+}$ fragment was observed following electronic excitation with no protonated $H^+(H_2O)_n$ water clusters detected.[22,24] Another point is related to the established trend in the spectral shift of the OH stretching to higher frequency with increasing the proton affinity (PA) of the proton donor.[30] Although the PA of the phenyl radical (211 kcal/mol)[31] is much larger than that of water (165 kcal/mol),[31] methanol (180 kcal/mol),[31] and dimethyl ether (189 kcal/mol),[31] the band position of the $(C_6H_6^{\bullet+})(H_2O)_4$ cluster [presumably $(C_6H_5^{\bullet})H^+(H_2O)_4$] where the proton donor is the phenyl radical is similar to the band position of the $(H_2O)H^+(H_2O)_4$ cluster where the proton donor is a water molecule.[22] In summary, it is not very clear from the spectroscopic studies whether the proton in these clusters is located on the benzene moiety ($C_6H_5^{\bullet}H^+$) or in the attached water cluster ($H^+(H_2O)_n$). This may result from the various methods that generate the cluster ions and whether they provide the energy requirements for proton transfer in the clusters.

To provide detailed energetics and kinetics of the proton transfer reaction in the $(C_6H_6^{\bullet+})(H_2O)_n$ cations, we studied the stepwise hydration and deprotonation of the benzene radical cations in the gas phase under thermal conditions.[32] In this paper, we provide a detailed experimental and theoretical study of the energetics and structures of the hydrated ions $(C_6H_6^{\bullet+})(H_2O)_n$ and the proton transfer products $(C_6H_5^{\bullet})H^+(H_2O)_n$, along with the temperature dependence and the mechanism of the reaction. We also compare the current gas phase results obtained under well-defined thermal conditions with the spectroscopic studies of the $(C_6H_6^{\bullet+})(H_2O)_n$ cluster cations. This work aims to establish a unified molecular level understanding of the role of hydrogen bonding interactions in determining the structures of the hydrated ions and the mechanism of the overall deprotonation reaction.

II. Experimental Section

The experiments were performed using the VCU mass-selected ion mobility spectrometer. The details of the instrument can be found in several publications, and only a brief description of the experimental procedure is given here.[33−35]

Mass-selected $C_6H_6^{\bullet+}$ ions (generated by electron impact ionization of benzene vapor) are injected (in 5−15 μs pulses) into the drift cell[33] (the inner diameter and length of the total cell are 8.1 and 8.9 cm, respectively) containing 0.2−0.3 Torr of pure H_2O or D_2O vapor. Flow controllers (MKS # 1479A) are used to maintain a constant pressure inside the drift cell. The temperature of the drift cell can be controlled

(15) Zwier, T. S. *Annu. Rev. Phys. Chem.* **1996**, *47*, 205−241.
(16) Gruenloh, C. J.; Carney, J. R.; Arrington, C. A.; Zwier, T. S.; Fredericks, S. Y.; Jordan, K. D. *Science* **1997**, *276*, 1678−1681.
(17) Gruenloh, C. J.; Carney, J. R.; Hagemeister, F. C.; Arrington, C. A.; Zwier, T. S.; Fredericks, S. Y.; Wood, J. T., III; Jordan, K. D. *J. Chem. Phys.* **1998**, *109*, 6601−6614.
(18) Tarakeshwar, P.; Choi, H. S.; Lee, S. J.; Lee, J. Y.; Kim, K. S.; Ha, T.-K.; Jang, J. H.; Lee, J. G.; Lee, H. *J. Chem. Phys.* **1999**, *111*, 5838−5850.
(19) Courty, A.; Mons, M.; Le Calve, J.; Piuzzi, F.; Dimicoli, I. *J. Phys. Chem. A* **1997**, *101*, 1445−1450.
(20) Solca, N.; Dopfer, O. *Chem. Phys. Lett.* **2001**, *347*, 59−64.
(21) Miyazaki, M.; Fujii, A.; Ebata, T.; Mikami, N. *Chem. Phys. Lett.* **2001**, *349*, 431−436.
(22) Miyazaki, M.; Fujii, A.; Ebata, T.; Mikami, N. *Phys. Chem. Chem. Phys.* **2003**, *5*, 1137−1148.
(23) Solca, N.; Dopfer, O. *J. Phys. Chem. A* **2003**, *107*, 4046−4055.
(24) Miyazaki, M.; Fujii, A.; Mikami, N. *J. Phys. Chem. A* **2004**, *108*, 8269−8272.
(25) Miyazaki, M.; Fujii, A.; Ebata, T.; Mikami, N. *J. Phys. Chem. A* **2004**, *108*, 10656−10660.
(26) Miyazaki, M.; Fujii, A.; Ebata, T.; Mikami, N. *Chem. Phys. Lett.* **2004**, *399*, 412−416.
(27) Wei, S.; Shi, Z.; Castleman, A. W., Jr. *J. Chem. Phys.* **1991**, *94*, 3268−3270 and references therein.
(28) Miyazaki, M.; Fujii, A.; Ebata, T.; Mikami, N. *Science* **2004**, *304*, 1134−1137.
(29) Shin, J. W.; Hammer, N. I.; Diken, E. G.; Johnson, M. A.; Walters, R. S.; Jaeger, T. D.; Duncan, M. A.; Christie, R. A.; Jordan, K. D. *Science* **2004**, *304*, 1137−1141.
(30) Wu, C. C.; Jiang, J. C.; Boo, D. W.; Lin, S. H.; Lee, Y. T.; Chang, H. C. *J. Chem. Phys.* **2000**, *112*, 176−188.
(31) Linstrom, P. J.; Mallard, W. G. *NIST Chemistry WebBook, NIST Standard Reference Database Number 69*; National Institute of Standards and Technology: Gaithersburg MD, 20899 (http://webbook.nist.gov) March 2003.
(32) Ibrahim, Y.; Alsharaeh, E.; Dias, K.; Meot-Ner, M.; El-Shall, M. S. *J. Am. Chem. Soc.* **2004**, *126*, 12766−12767.
(33) Rusyniak, M.; Ibrahim, Y.; Alsharaeh, E.; Meot-Ner, M.; El-Shall, M. S. *J. Phys. Chem. A* **2003**, *107*, 7656−7666.
(34) Rusyniak, M. J.; Ibrahim, Y. M.; Wright, D. L.; Khanna, S. N.; El-Shall, M. S. *J. Am. Chem. Soc.* **2003**, *125*, 12001−12013.
(35) Ibrahim, Y.; Alsharaeh, E.; Rusyniak, M.; Watson, S.; Meot-Ner, M.; El-Shall, M. S. *Chem. Phys. Lett.* **2003**, *380*, 21−28.

to better than ±1 K using six temperature controllers. Liquid nitrogen flowing through solenoid valves is used to cool the drift cell. The reaction products can be identified by scanning a second quadrupole mass filter located coaxially after the drift cell. The arrival time distributions (ATD) are collected by monitoring the intensity of each ion as a function of time. The reaction time can be varied by varying the drift voltage. The injection energies used in the experiments (5−20 eV, laboratory frame) are slightly above the minimum energies required to introduce the ions into the cell against the H_2O flow. Most of the ion thermalization occurs outside the cell entrance by collisions with the water vapor escaping from the cell entrance orifice. The ATDs of the injected $C_6H_6^{\bullet+}$ and the $(C_6H_6^{\bullet+})(H_2O)_n$ formed inside the cell are measured as a function of the drift voltage across the cell. The ion intensity ratio $(C_6H_6^{\bullet+})(H_2O)_n/(C_6H_6^{\bullet+})(H_2O)_{n-1}$ is measured from the integrated peak areas of the ATDs as a function of decreasing cell drift field corresponding to increasing reaction time, and equilibrium is achieved when a constant ratio is obtained. Equilibrium constants are then calculated from $K = [I(BzA_n^+)/I(BzA_{n-1}^+)P(A)]$, where I is the integrated ion intensity taken from the ATD and $P(A)$ is the partial pressure of the neutral A in the drift cell. A good test of equilibrium is the observation of identical ATDs of the reactant and product ions. If the $(C_6H_6^{\bullet+})(H_2O)_{n-1}$ and $(C_6H_6^{\bullet+})(H_2O)_n$ ions are in equilibrium, their ATDs must be identical.[33,35] All of the equilibrium experiments at different temperatures are conducted at correspondingly low drift fields and long residence times. The measured equilibrium constant is independent of the applied field across the drift cell in the low field region. The equilibrium constant measured as a function of temperature yields $\Delta H°$ and $\Delta S°$ from the van't Hoff equation [$\ln K = -\Delta H°/RT + \Delta S°/R$]. All of the results were reproduced at least three times. Pseudo-first-order rate constants were calculated using $\ln(I/I_0) = -kt$, where I is the integrated intensity of the ATD of the reactant ion $(C_6H_6^{\bullet+})$, I_0 is sum of the intensities of the reactant and all product ATD peaks including secondary products, and t is the mean drift time taken as the center of the ATD of the reactant ion.

III. Theoretical Calculations

Ab initio calculations were carried out with the GAUSSIAN03 software.[36] Equilibrium structures were obtained by full geometry optimization at the ROHF/6-31+G** level (all electrons are restricted to pairs except one). Energies were also calculated at the MP2//ROHF/6-31+G** level (single point MP2 calculation at the ROHF/6-31+G** optimized geometry). Binding energies were corrected for basis set superposition error (BSSE) by the counterpoise procedure.[37] Unscaled zero-point vibrational energy (ZPVE) was also included as described in the Results section.

IV. Results and Discussion

1. Mass Spectra, Arrival Time Distributions, and Equilibrium Measurements. Figure 1 displays a comparison of the product distributions after the injection of $C_6H_6^{\bullet+}$ into pure H_2O vapor at 288 and 239 K (the lowest achievable temperature because of the freezing of the water). At 288 K, the hydrated benzene ion, $C_6H_6^{\bullet+}(H_2O)$, and the protonated water pentamer, $(H_2O)_5H^+$, are the major ions observed. The minor FW_4 at 288 K corresponds to the hydrated benzene fragment, $C_4H_4^{\bullet+}(H_2O)_4$, $m/z = 124$. At lower temperatures, the smaller $C_6H_6^{\bullet+}(H_2O)_n$ ($n = 1, 2$) benzene−water clusters would be expected to disappear as the population shifts to higher clusters, following the usual trends in clustering series. However, the mass spectrum in the lower portion of Figure 1 shows that this is not the case. Rather, the $C_6H_6^{\bullet+}(H_2O)_n$ benzene−water clusters are divided into two groups with an intensity dip at $C_6H_6^{\bullet+}(H_2O)_3$. Protonated $(H_2O)_nH^+$ water clusters are also observed, and their distribution follows the usual continuous pattern.

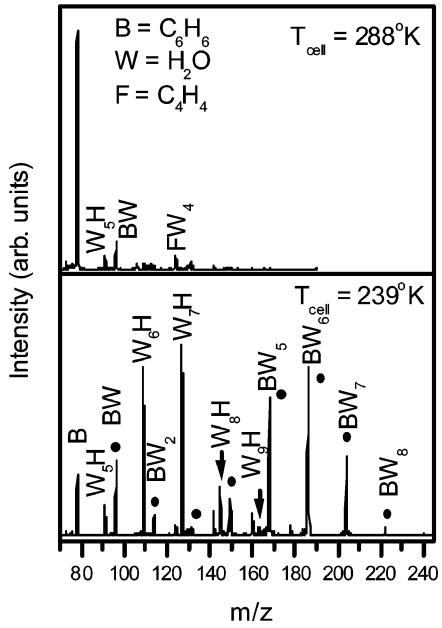

Figure 1. Benzene ions injected into (200 mTorr at 288 K and 120 mTorr at 239 K) pure H_2O at 13 eV injection energy and 25 V drift voltage. The minor FW_4 at 288 K corresponds to the hydrated $C_4H_4^+(H_2O)_4$ benzene fragment, $m/z = 124$. At 239 K, note the two groups of BW_n clusters with a dip at BW_3, compared with usual continuous distribution of the W_nH protonated water clusters.

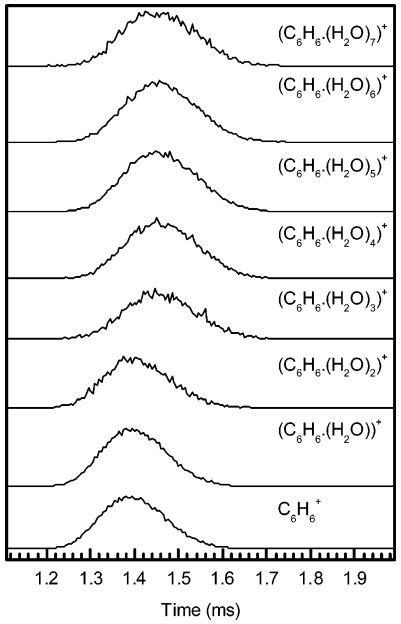

Figure 2. ATDs of $C_6H_6^{\bullet+}(H_2O)_n$ clusters obtained by injecting $C_6H_6^{\bullet+}$ at 13 eV (lab) into 199 mTorr of H_2O vapor and 25 V drift voltage at 248 K.

The division into the same two groups appears also in the ATDs shown in Figure 2. The $C_6H_6^{\bullet+}(H_2O)_n$ clusters with $n = 0-2$ have equal ATDs, and those with $n = 3-8$ have equal but longer arrival times. These ATDs indicate that ions in each group are coupled by equilibria according to the association reaction 1, but the two groups are not in equilibrium with each other. The ions in the higher mass group have slightly longer ATDs and smaller mobilities consistent with their larger masses

(36) Frisch, M. J. et al. *Gaussian 03*, revision C.02; Gaussian, Inc.: Pittsburgh, PA, 2004.
(37) Boys, S. F.; Bernardi, F. *Mol. Phys.* **1970**, *19*, 553−561.

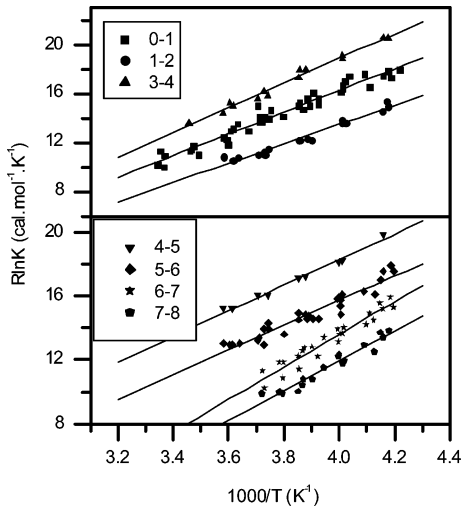

Figure 3. van't Hoff plots for the $C_6H_6^{\bullet+}(H_2O)_{n-1} + H_2O \leftrightarrow C_6H_6^{\bullet+}(H_2O)_n$ reactions for $n - 1$ and n as indicated.

Table 1. Measured Thermochemistry ($\Delta H°_{n-1,n}$ and $\Delta S°_{n-1,n}$) of Clustering Reactions 1, and Calculated Binding Energies (ΔE) at the MP2//ROHF/6-31+G** Level Corrected for ZPE and BSSE[a]

	Clustering equilibrium (1)		
n	$\Delta H°_{n-1,n}$	$\Delta S°_{n-1,n}$	ΔE
1	−9.0	−19.5	−8.5
2	−8.0	−18.9	−7.6
3	−8[b]		−7.8
4	−10.3	−22.4	−7.5
5	−8.6	−18.1	
6	−7.8	−15.1	
7	−9.8	−25.5	
8	−11.1	−32.6	

[a] Units are kcal/mol; estimated error: $\Delta H°$ ±1 kcal mol^{-1}, $\Delta S°$ ±3 cal mol^{-1} K^{-1}. [b] Estimated based on $n = 2$ binding energy.

and cross sections. We attribute the separation into two groups to the deprotonation side reaction (Associative/Proton Transfer/Dissociative (APTD), reaction 2) that depletes the $C_6H_6^{\bullet+}(H_2O)_3$ ion and, therefore, perturbs the equilibrium between $C_6H_6^{\bullet+}(H_2O)_2$ and $C_6H_6^{\bullet+}(H_2O)_3$, as discussed below.

Association:

$$C_6H_6^{\bullet+}(H_2O)_{n-1} + H_2O \leftrightarrow C_6H_6^{\bullet+}(H_2O)_n \qquad (1)$$

Associative/Proton Transfer/Dissociative (APTD):

$$C_6H_6^{\bullet+}(H_2O)_{n-1} + H_2O \rightarrow (H_2O)_nH^+ + C_6H_5^{\bullet} \qquad (2)$$

2. Binding Energies and Thermochemistry. The equilibrium constants for the stepwise hydration of $C_6H_6^{\bullet+}$ (reaction 1) yielded the van't Hoff plots shown in Figure 3. The resulting $\Delta H°$ and $\Delta S°$ values, along with the calculated ab initio binding energies of the $C_6H_6^{\bullet+}(H_2O)_n$ clusters, are listed in Table 1. We also performed the equilibrium constant measurements using D_2O vapor and obtained the same $\Delta H°$ values as for H_2O, that is, the isotope effect is smaller than the experimental accuracy of ±1 kcal mol^{-1}.

We could not measure the 2,3 equilibrium due to the depletion of the $C_6H_6^{\bullet+}(H_2O)_3$ ion by the APTD reaction (reaction 2). The experiment-based thermochemistry listed in Table 2 indicates that this reaction becomes thermoneutral at $n = 4$, and therefore, it can deplete the $n = 3$ ion. This can perturb the 2,3 equilibrium and prevent equilibrium coupling of the $n = 0-2$ and $3-8$ groups, leading to the observed grouping of the ATDs shown in Figure 2. In such cases, where the equilibrium is perturbed by side reactions, the perturbation depends on the rate of these reactions versus the rate at which equilibrium is achieved.[38] Equilibrium is generally achieved faster in higher association steps because of faster association in the larger clusters with more degrees of freedom. Correspondingly, the equal ATDs of the $n = 3-8$ clusters shown in Figure 2 indicate that the equilibrium is not perturbed significantly by the deprotonation reaction.

Table 2. $\Delta H°_{n-1,n}$ of Reaction 2, and Calculated $\Delta E_{n-1,n}$ at the MP2//ROHF/6-31+G** Level Corrected for ZPE[a]

	(APTD, Reaction 2) $C_6H_6^{\bullet+}(H_2O)_{n-1} + H_2O \rightarrow C_6H_5^{\bullet} + (H_2O)_nH^+$	
n	$\Delta H°_{n-1,n}$[b]	$\Delta E_{n-1,n}$
1	46	48.9
2	23	24.5
3	10	11.9
4	0	2.4
5	−3	
6	−5	
7	−8	
8	−8	

[a] Units are kcal/mol. [b] Experiment-based values using experimental binding energy from reaction 1 and $(H_2O)_nH^+$ binding energies from NIST.[31]

The measured thermochemical values, shown in Table 1, are unusual in that the binding energies change little from $n - 1$, $n = 0,1-7,8$, unlike the usual regular decrease with n.[39] This could suggest that there are several binding sites with comparable energies for the water molecules to attach to the $C_6H_6^{\bullet+}$ cation. Another interesting result is the remarkable increase in the $-\Delta S°_{6,7}$ and $-\Delta S°_{7,8}$ values, which suggests strong orientational restraint of water in these larger clusters.[40] In fact, three-dimensional cage-like structures involving multiple rings sharing edges are the lowest energy conformers of the water heptamer and octamer.[17,40] The observed large negative entropy of the $Bz^{\bullet+}(H_2O)_8$ cluster may be consistent with the formation of a cage-like structure by 8 H_2O molecules similar to neutral water clusters.[17,40]

The measured binding energies agree well with the calculated ab initio binding energies (MP2 + ZPE + BSSE), except for the 3,4 equilibrium. The experimental result may be perturbed by reaction 2, and the calculations may require full inclusion of electron correlation to capture most the details of the interactions between four water molecules and the $C_6H_6^{\bullet+}$ cation. Also, the experiment-based thermochemistry of reaction 2 is correctly predicted by the ab initio calculations, as shown in Table 2.

3. Calculated Structures of the Hydrated Benzene$^{\bullet+}$ Cations. The calculated structures of the lowest energy isomers that we have found for the $C_6H_6^{\bullet+}(H_2O)_n$ clusters are shown in Figure 4. Figure 5 displays the structures of other low energy isomers found that have comparable energies. The following discussion concerns the lowest energy structures of the selected initial structures investigated in this work.

$C_6H_6^{\bullet+}(H_2O)$. For the $n = 1$ cluster, the lowest energy isomer has a bifurcated structure with H_2O bonding to two CH

(38) Meot-Ner (Mautner), M.; Sieck, L. W. *Int. J. Mass Spectrom. Ion Processes* **1991**, *109*, 187−208.
(39) Meot-Ner (Mautner), M. *J. Am. Chem. Soc.* **1984**, *106*, 1257−1264.
(40) Ludwig, R. *Angew. Chem., Int. Ed.* **2001**, *40*, 1808−1827.

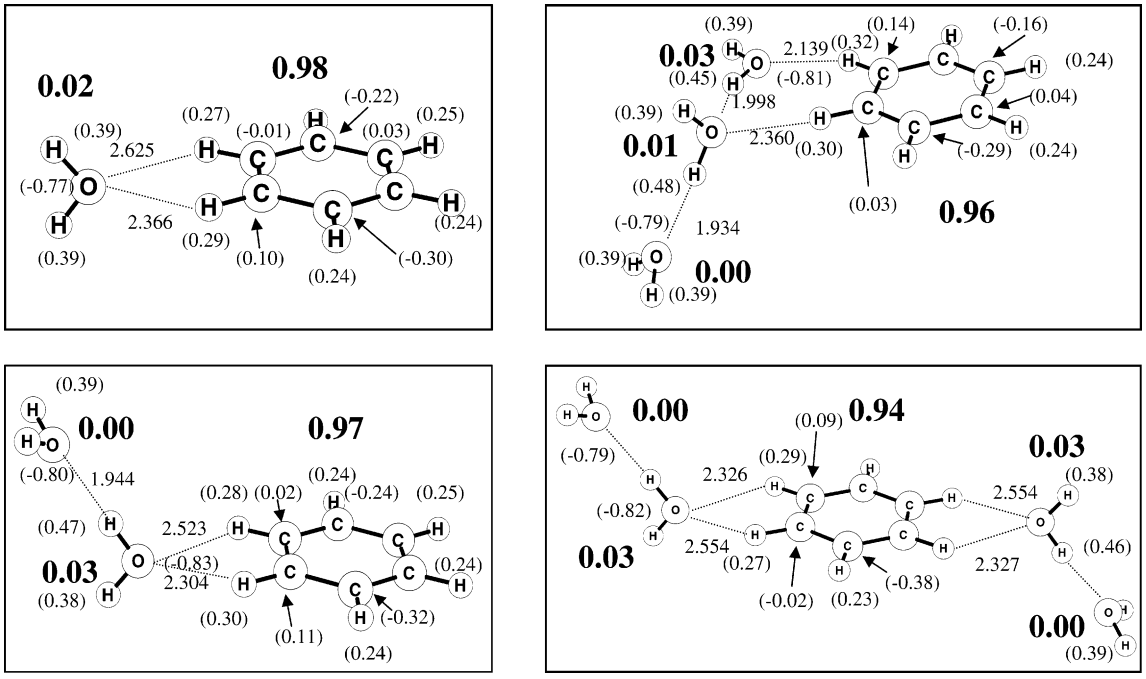

Figure 4. Equilibrium geometries for $C_6H_6^{\bullet+}(H_2O)_{1-4}$ clusters at the ROHF/6-31+G** level. Bond lengths are in angstroms, while the molecular charges are in bold and atomic charges are in parentheses.

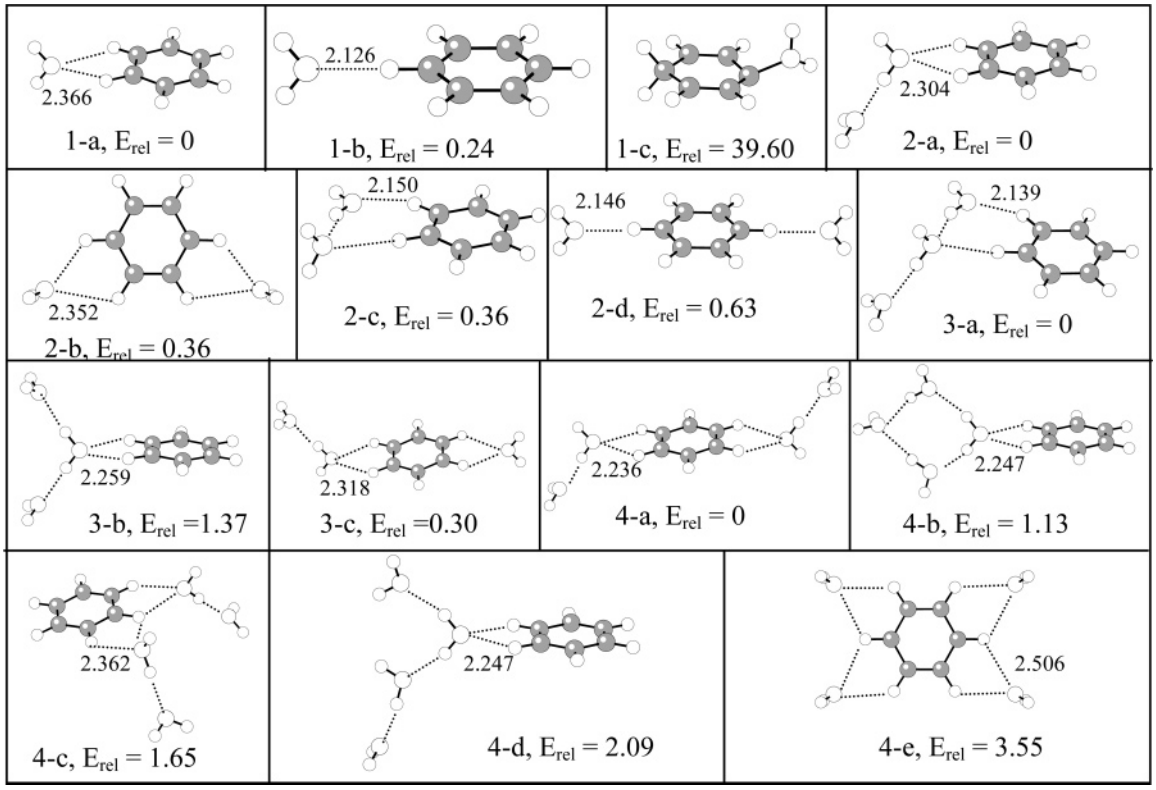

Figure 5. Different structures of $C_6H_6^{+}(H_2O)_{1-4}$ optimized at the ROHF/6-31+G** level. E_{rel} is the energy (kcal mol^{-1}) relative to the most stable isomer for each *n*. The binding energies of the most stable isomers (a) are given in Table 1.

hydrogens, as shown in Figure 4. This was also found in previous ab initio studies.[20−23,41,42] The MP2-corrected binding energy of 8.5 kcal/mol (Table 1) matches well with the experimental value of 9.0 ± 1 kcal/mol and that reported from the IR photodissociation experiment of 9.4 ± 0.3 kcal/mol.[24] In this optimized geometry, 98% of the charge remains on the benzene ring (the charge density was calculated according to *Mulliken population analysis*).[36] The previously calculated binding energies at different levels of theory predicted values ranging from 9.4 to 13.7 kcal/mol.[20,21,41,42] Since our calculated binding energy agrees with the experiment, we consider that the MP2//ROHF/6-31+G** level is satisfactory.

The addition of the first H_2O molecule to $C_6H_6^{\bullet+}$ involves unconventional carbon-based $C-H^{\delta+}\cdots OH_2$ bonding (as shown

in Figure 4), and it is of interest to compare this with conventional $N-H^+\cdots OH_2$ bonds.[43] Ionic hydrogen bond strengths are also related to proton affinity differences (ΔPA) between the components.[39] In this case, we can compare an unconventional and conventional bond to H_2O by two donors of equal PAs. The present binding energy of $C_6H_5-H^{\bullet+}\cdots OH_2$ of 9.0 kcal mol^{-1} is smaller than that of $C_6H_5NH_3^+\cdots OH_2$ (15.1 kcal/mol),[31] although the hydrogen bond donor bases, $C_6H_5^\bullet$ and $C_6H_5NH_2$, have equal PAs (211 kcal/mol).[31] The $C-H^{\delta+}\cdots O$ hydrogen bonds are weaker possibly because the donor C−H bonds are harder to elongate for partial proton transfer to the ligand than are the $N-H^+$ bonds.[43]

The $C-H^{\delta+}\cdots OH_2$ bond strength seems to be similar in carbon-based ionic hydrogen bonds of various donors. For example, the bond strengths of $C_6H_6^{\bullet+}(H_2O)_n$, $n = 1$ and 2, are similar to those in $N(CH_3)_4^+(H_2O)_n$ clusters,[43] although the $C-H^{\delta+}$ donor is a radical ionized aromatic in the first system and even-electron aliphatic ion in the other.

The $C_6H_6^{\bullet+}(H_2O)$ adduct could have a covalent structure similar to that of protonated phenol plus a hydrogen on one of the benzene carbons (isomer 1-c in Figure 5). However, our ab initio calculations showed that this isomer has a much higher energy, by 39.6 kcal mol^{-1}, than that of the lowest energy hydrogen-bonded isomer 1-a because the formation of the tetrahedral carbons disrupts the aromatic ring. Another isomer of the covalent ion, where the OH_2 and H are bonded to the sp^3 carbon, did not result in a minimum in the calculations. Another test of this structure is the binding energy of the second H_2O molecule. Given the PA of phenol (195.3 kcal mol^{-1}) and hydrogen bond energy −ΔPA correlations,[39] the 1,2 binding energy would be 20−22 kcal mol^{-1}, much larger than the observed value of 8.0 kcal mol^{-1}. We, therefore, conclude that the covalent protonated phenol-type ion is not formed.

$C_6H_6^{\bullet+}(H_2O)_2$. The addition of the second water molecule forms an "*externally solvated*" structure (2-a in Figure 5) where the solvent molecules are bonded to each other and the ion is external to this solvent cluster. The calculated energy of this isomer is 0.6 kcal mol^{-1} lower than that of the "*internally solvated*" structure (2-d in Figure 5) in which both water molecules are bonded to the $C_6H_6^{\bullet+}$ ion, which is therefore "inside" the solvent. The hydrogen bond of 1.944 Å between the two water molecules in isomer 2-a is shorter than that between the first water molecule and the CH of the benzene ion (2.304 Å). The MP2-corrected binding energy is 7.6 kcal/mol, which agrees well within the experimental value of 8.0 ± 1 kcal/mol. With the addition of the second H_2O molecule, the $CH^{\delta+}\cdots O$ hydrogen bond becomes shorter and the charge shifts slightly more to water, although 97% is still retained on the core ion.

$C_6H_6^{\bullet+}(H_2O)_3$. The lowest energy structure of $C_6H_6^{\bullet+}(H_2O)_3$ is obtained when two water molecules solvate two *ortho*-CH hydrogens and the third water hydrogen bonds to one of these water molecules (Figure 4). A hydrogen bond between the two H_2O molecules attached to the benzene cation forms a cyclic structure which apparently further stabilizes the cluster. The charge on the benzene core ion decreases slightly to 96%. There is no net charge on the outer H_2O molecule, which should therefore hydrogen bond to further outer-sphere molecules with effectively neutral hydrogen bond strength. The hydrogen bonds to $C_6H_6^{\bullet+}$ are shorter again than in the $n = 1$ and 2 clusters.

$C_6H_6^{\bullet+}(H_2O)_4$. The lowest energy structure of $C_6H_6^{\bullet+}(H_2O)_4$ (Figure 4) is symmetrical with a water dimer on each side of the ion, both forming bifurcated bonds with the ion. The MP2-corrected binding energy of −7.5 kcal/mol is lower than the experimentally measured one of −10.3 ± 1.0 kcal/mol, which may be perturbed by reaction 2. The difference may also indicate that larger basis sets are needed to accurately describe the interactions in large clusters with four water molecules attached to the benzene cation or that there is another isomer that was not identified on the theoretical potential energy surface.

Unlike most clustering series, the donor C−H bond lengths remain constant in the 1.073−1.076 Å range with increasing cluster size, from $n = 1-4$. Detailed scrutiny of these covalent bond lengths indicates little correlation with the C−H bond lengths. This insensitivity of R(C−H) to H-bond formation is consistent with earlier work which indicates that sp^2-hybridized CH typically undergoes only very minor bond length changes in such situations.[44] Similarly, the charge on the primary hydrogen bonding proton of $C_6H_6^{\bullet+}$ (shortest H-bond) in the bifurcated isomers 1-a through 4-a in Figure 5 changes little, from 0.29 at $n = 1$ to 0.30 in the $n = 2-4$ clusters. These trends indicate little partial proton transfer to water in the clusters, suggesting a barrier for deprotonation.

With respect to deprotonation, isomer 4-b in Figure 5 may be relevant. This isomer is only 1.1 kcal/mol higher in energy than isomer 4-a. In isomer 4-b, all the water molecules are bonded together, which allows pulling the proton from $C_6H_6^{\bullet+}$. With increasing *n*, the shortest hydrogen bond in each cluster becomes shorter, from 2.366 → 2.304 → 2.259 → 2.247 Å in the bifurcated externally solvated isomers (1-a through 4-a, respectively), toward the 2.218 Å in the product-like transition state that we calculated for $C_6H_6^{\bullet+}(H_2O)_4$, consistent with the decreasing energy of the barrier with increasing *n* as discussed below.

In summary, the hydrogen bond shortens, but the C−H bond length, charge on the donor proton, and binding energies change little with increasing *n*. This is different from conventional $OH^+\cdots O$ and $NH^+\cdots O$ bonds that can transfer a proton increasingly to more effective acceptors, toward full proton transfer. The $C-H^{\delta+}$ donors do not develop partial proton transfer efficiently in the clusters, suggesting that a barrier must be overcome eventually for full deprotonation.

"Internally" and "Externally" Solvated Structures. It is of interest to compare "*internally solvated*" structures, where the inner solvent molecules are bonded directly to the ion, with "*externally solvated*" structures, where the ion is hydrogen bonded to the exterior of a solvent cluster. For the $n = 2$ cluster, the energies of the internally solvated isomers 2-b, 2-c, and 2-d, shown in Figure 5, are comparable to that of the externally solvated isomer 2-a, with the latter being slightly more stable. Miyazaki et al.[21] found spectroscopic evidence for both types of isomers, whose ratio depended on the conditions of the cluster formation. For the $n = 3$, only externally solvated structures were obtained by ab initio calculations. In the $n = 4$ cluster, isomer 4-a, the two $(H_2O)_2$ groups are attached to two benzene

(41) Tachikawa, H.; Igarashi, M.; Ishibashi, T. *Phys. Chem. Chem. Phys.* **2001**, *3*, 3052−3056.
(42) Tachikawa, H.; Igarashi, M. *J. Phys. Chem. A* **1998**, *102*, 8648−8656.
(43) Meot-Ner (Mautner), M.; Deakyne, C. A. *J. Am. Chem. Soc.* **1985**, *107*, 474−479.
(44) Scheiner, S.; Kar, T. *J. Phys. Chem. A* **2002**, *106*, 1784−1789.

Table 3. Calculated $\Delta E_{n-1,n}$ for Reactions 3−7 at the MP2//ROHF/6-31+G** Level Corrected for ZPE[a]

	IPT, Reaction 3 $C_6H_6^{\bullet+}(H_2O)_n \rightarrow C_6H_5^{\bullet}(H_2O)_nH^+$	DIPT, Reaction 4 $C_6H_6^{\bullet+}(H_2O)_n \rightarrow C_6H_5^{\bullet} + (H_2O)_nH^+$	AIPT, Reaction 5 $C_6H_6^{\bullet+}(H_2O)_{n-1} + H_2O \rightarrow C_6H_5^{\bullet}(H_2O)_nH^+$	Reaction 6[b] $C_6H_5^{\bullet}(H_2O)_{n-1}H^+ + H_2O \rightarrow C_6H_5^{\bullet}(H_2O)_nH^+$	Reaction 7 $C_6H_5^{\bullet} + (H_2O)_nH^+ \rightarrow C_6H_5^{\bullet}(H_2O)_nH^+$
n	$\Delta E_{n-1,n}$	$\Delta E_{n-1,n}$	$\Delta E_{n-1,n}$	$\Delta E_{n-1,n}$	$\Delta E_{n-1,n}$
1	37.3	58.8	27.4	−19.4	−21.5
2	20.1	33.7	10.9	−23.6	−13.6
3	9.1	21.2	−0.3	−17.7	−12.1
4	3.1	11.5	−5.9	−12.8	−8.4

[a] Units are kcal/mol. [b] MP2 + ZPE + BSSE.

hydrogens, containing features of both internal and external solvation. This isomer has energy significantly lower than those of the purely internally (isomer 4-e) or purely externally (isomer 4-d) solvated isomers, as shown in Figure 5. Note that all of the $n = 1-4$ solvation states have isomers within about 1 kcal/mol of the lowest energy structure, and these isomers may be in equilibrium in the observed clusters.

It is notable that in all of the $C_6H_6^{\bullet+}(H_2O)_n$ ($n = 1-4$) clusters, water is bonded to $C_6H_6^{\bullet+}$ by two hydrogen bonds whose lengths differ by about 0.25 Å. This feature remains even after proton transfer in the $C_6H_5^{\bullet}(H_2O)_4H^+$ cluster as shown below.

4. Energies of the Proton Transfer and Intracluster Reactions. In addition to reactions 1 and 2, the experimental data and the ab initio calculations can be used to calculate the energies of the following reactions.

Intracluster Proton Transfer (IPT):

$$C_6H_6^{\bullet+}(H_2O)_n \rightarrow C_6H_5^{\bullet}(H_2O)_nH^+ \quad (3)$$

Dissociative Intracluster Proton Transfer (DIPT):

$$C_6H_6^{\bullet+}(H_2O)_n \rightarrow (H_2O)_nH^+ + C_6H_5^{\bullet} \quad (4)$$

Associative Intracluster Proton Transfer (AIPT):

$$C_6H_6^{\bullet+}(H_2O)_{n-1} + H_2O \rightarrow C_6H_5^{\bullet}(H_2O)_nH^+ \quad (5)$$

H_2O Binding to $C_6H_5^{\bullet}(H_2O)_nH^+$ clusters following PT:

$$C_6H_5^{\bullet}(H_2O)_{n-1}H^+ + H_2O \rightarrow C_6H_5^{\bullet}(H_2O)_nH^+ \quad (6)$$

$C_6H_5^{\bullet}$ Binding to Protonated Water Clusters:

$$C_6H_5^{\bullet} + (H_2O)_nH^+ \rightarrow C_6H_5^{\bullet}(H_2O)_nH^+ \quad (7)$$

$C_6H_6^{\bullet+}$ Binding to Water Clusters:

$$C_6H_6^{\bullet+} + (H_2O)_n \rightarrow C_6H_6^{\bullet+}(H_2O)_n \quad (8)$$

Proton Transfer to Water Clusters:

$$C_6H_6^{\bullet+} + (H_2O)_n \rightarrow (H_2O)_nH^+ + C_6H_5^{\bullet} \quad (9)$$

The ab initio energies of reactions 3−7 are included in Table 3, and the $\Delta H°$ values for reactions 8 and 9 (calculated on the basis of the experimental binding energies in Table 1) are listed in Table 4.

Reactions 3 and 4 represent intracluster proton transfer (IPT) and dissociative intracluster proton transfer (DIPT) reactions, respectively. Reaction 5 represents association followed by intracluster proton transfer (AIPT). The IPT reaction 3 remains endothermic at least to $n = 4$, but the AIPT reaction 5 is more favorable because the binding energy of the incoming H_2O molecule adds to the exothermicity. For similar reasons, although the direct DIPT reaction 4 remains endothermic at any cluster size, the APTD reaction 2 becomes energetically feasible at $n = 4$, and it seems to be the reaction observed in our experiments as discussed below.

Table 4. $\Delta H°_{n-1,n}$ of Association of $C_6H_6^{\bullet+}$ (Reaction 8) and Proton Transfer (Reaction 9) to Preformed Water Clusters[a]

	(Reaction 8)[b] $C_6H_6^{\bullet+} + (H_2O)_n \rightarrow C_6H_6^{\bullet+}(H_2O)_n$	(Reaction 9)[b,c] $C_6H_6^{\bullet+} + (H_2O)_n \rightarrow (H_2O)_nH^+ + C_6H_5^{\bullet}$
n	$\Delta H°_{n-1,n}$	$\Delta H°_{n-1,n}$
1	−9	46
2	−14	17
3	−17	1
4	−19	−11
5	−21	−17
6	−21	−20
7	−22	−22
8	−23	−22

[a] Units are kcal/mol. [b] From experimental binding energies of $C_6H_6^{\bullet+}(H_2O)_n$ for n =1, 2, and 5−8 and ab initio binding energies for $n = 3$ and 4. For the $(H_2O)_n$ clusters, we used the following stepwise binding energies ($\Delta H°_{n-1,n}$): 3,[23] 5,[49] 6, 7, 8, 9, 10. Values for $n = 4-8$ estimated from approach to macroscopic $\Delta H°_{vap} = 10.5$ kcal/mol. [c] Calculated using selected $-\Delta H°_{n-1,n}$ values for $(H_2O)_nH^+$ clusters, $n = 2-8$ as follows: −32, −21, −18, −13, −11, −11, −10, −10 kcal/mol from NIST.[31]

Reaction 6 gives the binding energies of H_2O molecules to the $C_6H_5^{\bullet}(H_2O)_nH^+$ clusters following proton transfer. Reaction 7 gives the binding energies of $C_6H_5^{\bullet}$ to protonated water clusters $(H_2O)_nH^+$, which are smaller than the respective binding energies of H_2O molecules to the $(H_2O)_nH^+$ clusters. For example, the binding energies of $C_6H_5^{\bullet}$ to the $n = 1-3$ $(H_2O)_nH^+$ clusters are 21.5, 13.6, and 12.1 kcal mol^{-1}, while the binding energies of an H_2O molecule to these clusters are 32, 21, and 18 kcal mol^{-1}, respectively.[31] The less polar $C_6H_5^{\bullet}$ radical is a weaker ligand, although it is more polarizable and has a carbon lone pair hydrogen bond acceptor. In particular, the dipole moment of this radical is computed to be 0.784 D (ROHF/6-31+G**), roughly $^1/_3$ of the 2.232 D calculated for H_2O. The relatively weak binding of $C_6H_5^{\bullet}$ to large $(H_2O)_nH^+$ clusters suggests that it would not perturb the structures of the $(H_2O)_nH^+$ clusters significantly, which is consistent with the similarity of the spectra of $(H_2O)_nH^+$ and $C_6H_5^{\bullet}(H_2O)_nH^+$ clusters for $n = 4-23$.[25]

From the experimental data, we can also calculate the binding energies of $C_6H_6^{\bullet+}$ to preformed water clusters $(H_2O)_n$ in reaction 8, as shown in Table 4. These energies should approach the solvation energy of $C_6H_6^{\bullet+}$ in bulk water at $n =$ infinity, which in turn can yield the ionization energy of benzene in liquid water. Solvation should reduce the ionization energy, and indeed, theoretical studies showed that the ionization energies of benzene and polycyclic aromatics are lowered by 1.5−2.1 eV in ice.[10,14]

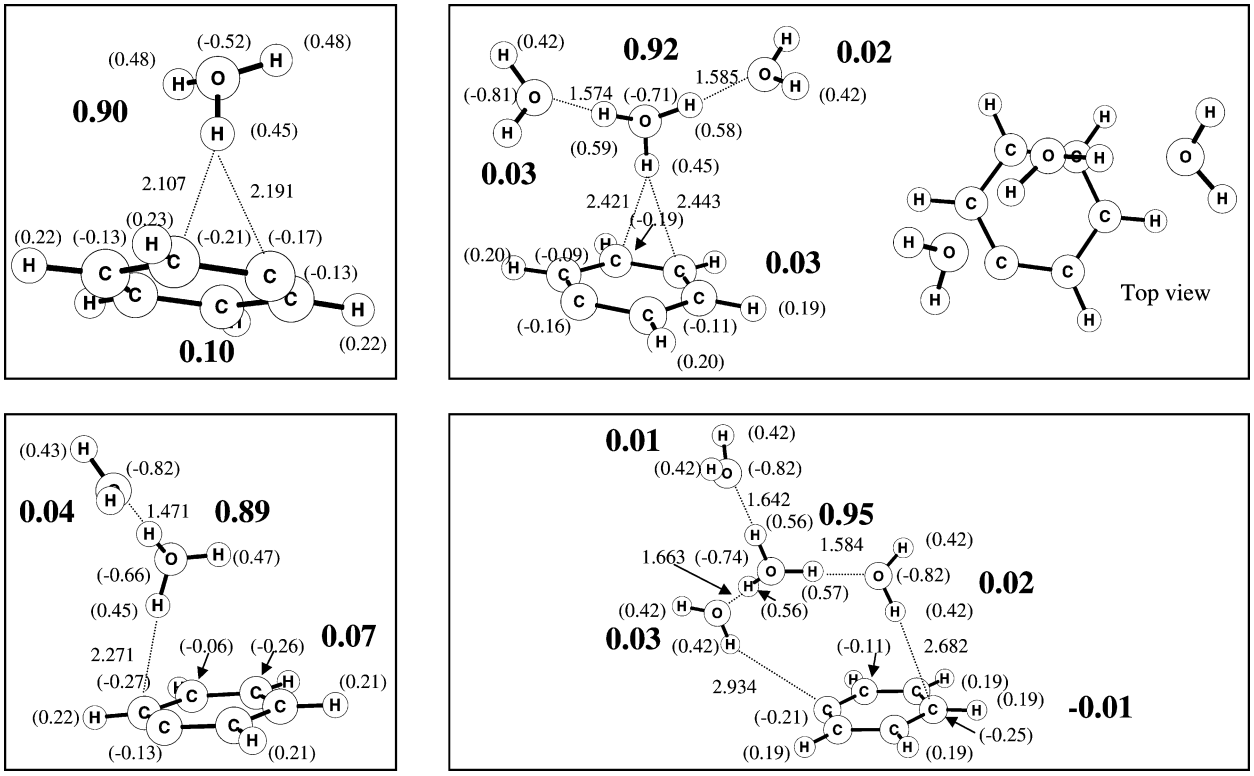

Figure 6. Equilibrium geometries for $C_6H_5^{\bullet}(H_2O)_{1-4}H^+$ clusters at the ROHF/6-31+G** level. Bond lengths are in angstroms, while the molecular charges are in bold and atomic charges are in parentheses.

Reaction 9 represents PT to a water cluster, for example, when the benzene$^{\bullet+}$ ion reacts with preformed water clusters in supersonic beam expansion or possibly in space. It is clear that the PT is significantly exothermic for $(H_2O)_n$ with $n \geq 4$.

5. Structures of the Proton-Transferred $C_6H_5^{\bullet}(H_2O)_nH^+$ Clusters. To study the proton transfer reaction, we optimized geometry of the $C_6H_5^{\bullet}(H_2O)H^+$ complex. As a starting point, we used the optimized geometry of $C_6H_6^{\bullet+}(H_2O)$, moved the proton away from the carbon ~1 Å from the H_2O oxygen, and allowed the structure to relax. Since the proton affinity of $C_6H_5^{\bullet}$ (211 kcal/mol) is higher than that of H_2O (165 kcal/mol), we expected that the proton would move back to the $C_6H_5^{\bullet}$. However, in the final lowest energy geometry, the proton stayed on H_3O^+ attached to $C_6H_5^{\bullet}$. Interestingly, 90% of the charge was transferred to H_3O^+, and it moved from the $C_6H_5^{\bullet}$ plane to a position above the plane. This repositioning may be simply understood in terms of the electrostatic part of the interaction. The quadrupole moment of the $C_6H_5^{\bullet}$ radical is positive in this unit's molecular plane, but negative above and below. It is thus natural for the positively charged H_3O^+ to move out of the plane.

The calculated structures of lowest energy PT $C_6H_5^{\bullet}H^+(H_2O)_n$ ($n = 1-4$) clusters are shown in Figure 6. These structures reflect the stability of the H_3O^+ and its preferential solvation by water molecules. It also appears that the extent of hydrogen bonding interaction between H_3O^+ and the $C_6H_5^{\bullet}$ plane decreases as more water molecules are attached to H_3O^+. This is clearly reflected in the gradual increase of the OH···C distance between H_3O^+ and the $C_6H_5^{\bullet}$ from 2.107, 2.271, 2.421, to 2.682 Å in the $C_6H_5^{\bullet}H^+(H_2O)_n$ structures with $n = 1-4$, respectively, as shown in Figure 6.

Figure 7 displays the structures of other low energy isomers found for the $C_6H_5^{\bullet}H^+(H_2O)_n$ clusters with $n = 3$ and 4. The structures involving cyclic water tetramers (isomers 4′-c and 4′-d in Figure 7) have relatively higher energies (≈3 kcal/mol) compared to the lowest energy structure involving the closed-shell solvated hydronium ion $H_3O^+(H_2O)_3$ (isomer 4′-a). In comparison with that of the hydrated benzene cation, $C_6H_6^{\bullet+}(H_2O)_4$, the structure involving a cyclic water tetramer (isomer 4-b in Figure 5) is only 1 kcal/mol higher in energy than the lowest energy structure 4-a. This suggests that cyclic structures similar to neutral water clusters[41] are formed more readily in the hydrated clusters $C_6H_6^{\bullet+}(H_2O)_n$ than in the PT $C_6H_5^{\bullet}H^+(H_2O)_n$ clusters. This results because there is little charge on water in the $C_6H_6^{\bullet+}(H_2O)_n$ clusters and, therefore, they can develop structures similar to neutral water clusters.

6. H/D Exchange. Reaction 5 in Table 3 shows that associative intracluster PT is exothermic for $n \geq 3$. Intracluster PT in $C_6H_6^{\bullet+}(D_2O)_n$ would produce $C_6H_5^{\bullet}(D_2O)_nH^+$ clusters that are, in effect, $(D_2O)_nH^+$ clusters weakly hydrogen bonded to a $C_6H_5^{\bullet}$ radical. These $(D_2O)_nH^+$ centers should exchange a hydrogen readily with D_2O vapor leading to $C_6H_5^{\bullet}(D_2O)_nD^+$ clusters, one m/z unit higher than the original $C_6H_5^{\bullet}(D_2O)_nH^+$ ions. Nevertheless, the mass spectrum (given as Supporting Information) shows only the unexchanged clusters and not their $(m + 1)/z$ counterparts. Analogous results were obtained also by reverse labeling, when $C_6D_6^{\bullet+}$ was injected into H_2O vapor.

The lack of H/D exchange implies the absence of intracluster PT. To test this argument, these clusters can be compared with a system that contains an $N-H^+\cdots(OH_2)_n$ bond where no barrier to intracluster PT is expected. Correlated calculations have suggested that such a transfer would occur with no intervening energy barrier.[45] To keep other factors constant, we performed this test using 2-fluoropyridine $H^+(H_2O)_n$ clusters, as the C_5H_4-

(45) Yi, M.; Scheiner, S. *Chem. Phys. Lett.* **1996**, *262*, 567−572.

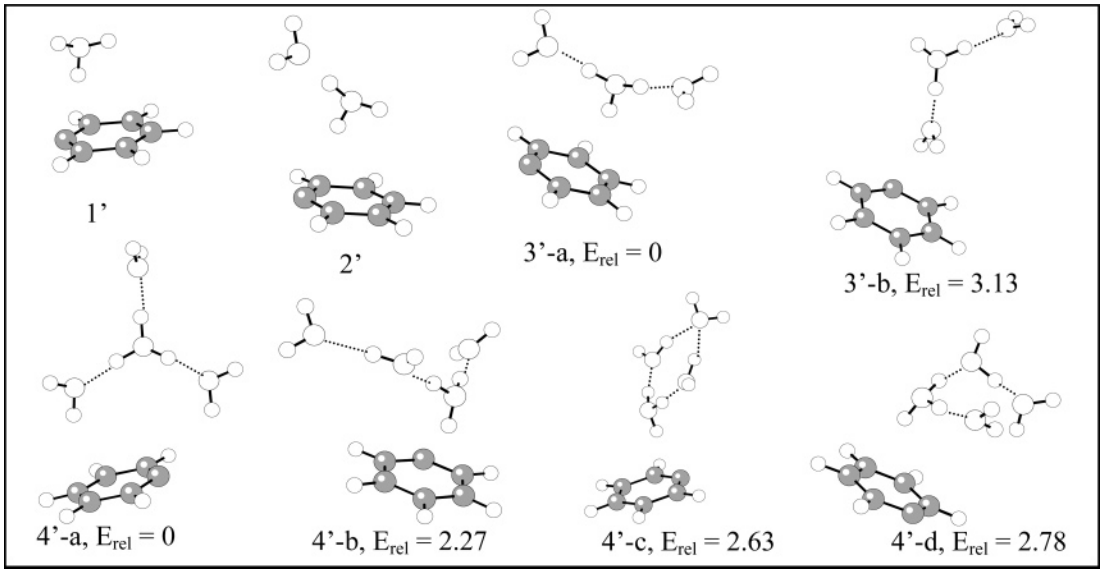

Figure 7. Different structures of $C_6H_5^{\bullet}(H_2O)_nH^+$ with $n = 1-4$ optimized at the ROHF/6-31+G** level. E_{rel} is the energy (kcal mol^{-1}) relative to the most stable isomer for each n. The binding energies of the most stable isomers are given in Table 1.

$FN-H^+$ donor bond is as strong as the $C_6H_5^{\bullet}-H^+$ donor bond (i.e., 2-fluoropyridine (C_5H_4FN) has a PA equal to that of $C_6H_5^{\bullet}$).[31] First, despite these PA relations, we calculated the bond strength of $C_5H_4FNH^+\cdots OH_2$ as 15.5 kcal mol^{-1}, while that of $C_6H_6^{\bullet+}\cdots OH_2$ is only 9.0 kcal mol^{-1}, confirming that the $N-H^+$ bond is indeed a more efficient donor. When $C_5H_4FN-D^+$ was injected into H_2O, it indeed formed $C_5H_4FN-D^+(H_2O)_n$ clusters that exchanged with H_2O to give $C_5H_4FN-H^+(H_2O)_n$ clusters, as shown in the Supporting Information.

The 2-fluoropyridine results demonstrate that when IPT transfer is possible, H/D exchange does occur. Therefore, the absence of H/D exchange of $C_6H_6^{\bullet+}(D_2O)_n$ with D_2O implies the absence of IPT under our conditions, even though it may be allowed energetically. This, in turn, suggests a barrier to the intracluster PT, which is supported by ab initio calculations below.

Note that the H/D exchange properties rule out *nondissociative intracluster PT* under our conditions but give no information about *dissociative PT*.

7. Barrier to Proton Transfer. The reverse IPT (reaction −3) is exothermic by 37.3 kcal/mol (at MP2 level) as indicated in Table 3. Nevertheless, the calculations show that the proton can remain on a shallow local minimum in the $C_6H_5^{\bullet}(H_3O^+)$ structure. The fact that the proton can stay at this position despite the highly exothermic reverse proton transfer indicates a significant energy barrier to proton transfer in the reverse, and therefore also in the forward direction. To find the barrier, the geometry of the transition state was optimized at the ROHF/6-31+G** level. At this level, the barrier for proton transfer in the $C_6H_6^{\bullet+}(H_2O)_n$ clusters is 42.5, 33.3, 28.2, and 26.1 kcal/mol for $n = 1-4$, respectively.

At the ROHF/6-31+G** level, the barrier for proton transfer from H_3O^+ back to $C_6H_5^{\bullet}$ is 3.1 kcal/mol. This explains why, in the calculations, the proton can remain at the local minimum of the $C_6H_5^{\bullet}(H_2O)H^+$ isomer. The second water molecule increased the back-barrier to 10.1 kcal/mol and lowered the endothermicity of the PT reaction to 23 kcal/mol which is still significant for the PT. The magnitude of this reverse transfer barrier grows along with the number of water molecules n. It is equal to 10, 16, and 20 kcal/mol for $n = 2$, 3, and 4, respectively. These reverse transfer barriers are affected by inclusion of zero-point vibrational energy, and even more so by inclusion of electron correlation which characteristically reduces proton transfer barriers. At the MP2//ROHF/6-31+G** level, and with ZPVE included, the reverse transfer barrier is reduced to 4 kcal/mol for $n = 3$ and 9 kcal/mol for $n = 4$; the barrier may disappear entirely for $n = 1$ and 2. However, a final resolution of this question would require the full reoptimization at the MP2 level of the geometries of the various minima, as well as the transition state to proton transfer, which is beyond the scope of these calculations.

The second water molecule is bonded to the H_3O^+ center more strongly than the first water molecule is bonded to phenyl hydrogen (Table 3, reaction 6). On subsequent addition of water molecules, a protonated water cluster started to evolve, still bound to the phenyl radical. The PT reaction became less endothermic but still not exothermic even for $n = 4$ (+3.1 kcal/mol, Table 3, reaction 3) with a barrier of 11.7 kcal/mol. As bonding in the $(H_2O)_nH^+$ center becomes stronger, bonding to $C_6H_5^{\bullet}$ becomes weaker, as shown in Table 3, reaction 7. This is also reflected in the hydrogen bond length which changes from ∼2.1 Å at $n = 1$ to ∼2.7 Å at $n = 4$ (Figure 6).

8. Kinetics and Mechanism of the Deprotonation of the Benzene$^{\bullet+}$ Cation. Figure 1 shows that $(H_2O)_nH^+$ clusters are formed upon the injection of $C_6H_6^{\bullet+}$ ions into H_2O vapor. Figure 8a shows that the total intensities of the $C_6H_6^{\bullet+}(H_2O)_n$ clusters decrease with increasing residence time in the drift cell, and that the rate increases with decreasing temperature. This shows that the overall deprotonation of $C_6H_6^{\bullet+}$ is a slow thermal reaction.

The time profiles, such as displayed in Figure 8a, allow calculating the pseudo-first-order rate coefficients for the overall reaction 2, with the total population of the $C_6H_6^{\bullet+}(H_2O)_n$ clusters that undergo this reaction, that is

$$k = -d\ln(\Sigma[C_6H_6^{\bullet+}(H_2O)_n]/\Sigma[C_6H_6^{\bullet+}(H_2O)_n] + \Sigma[H_2O_nH^+])$$

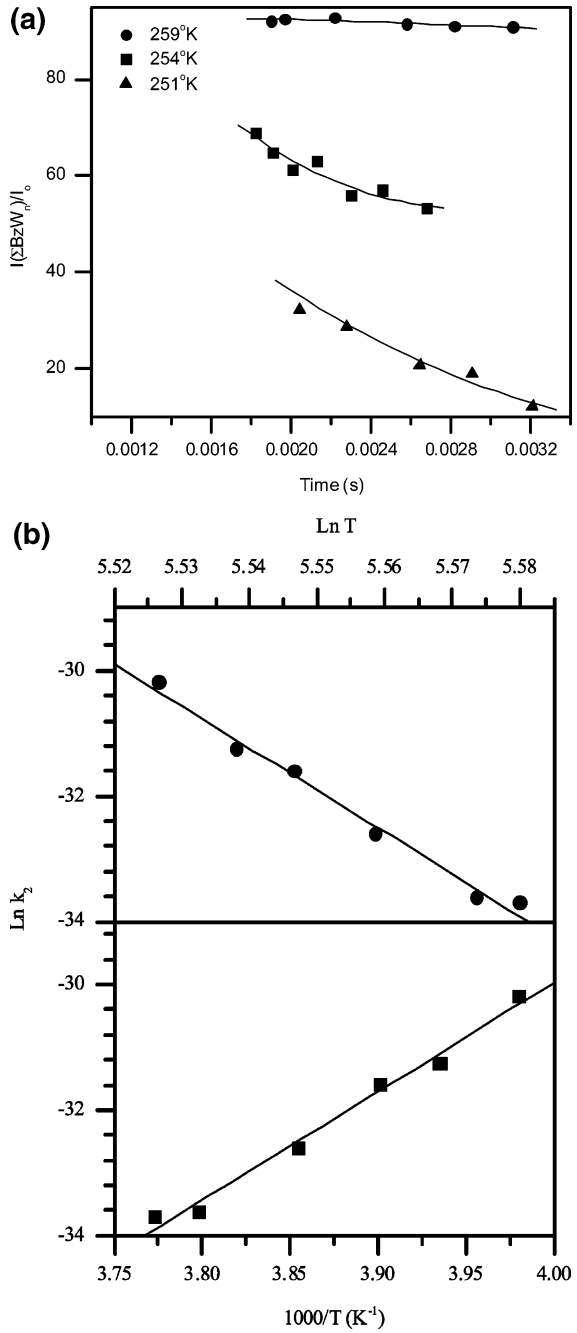

Figure 8. (a) Changes of the sums of intensities of the $C_6H_6^{\bullet+}(H_2O)_n$ group of ions with reaction time at several temperatures by injecting $C_6H_6^{\bullet+}$ using 17 eV (lab) into 300 mTorr H_2O. The reaction time was varied by varying the cell voltage between 2.0 and 3.4 V/cm and therefore the ATDs of the ions. The arrival time of each ion was considered the center of the ATD peak. (b) Temperature dependence of the pseudo-second-order rate coefficients for the overall conversion of the $C_6H_6^{\bullet+}(H_2O)_n$ group of hydrated benzene ion clusters to the $(H_2O)_nH^+$ group of protonated water clusters. The values of ln k are plotted versus ln T (K) corresponding to the $k = CT^{-n}$ form (top) and versus 1000/T (K) corresponding to the Arrhenius-type $k = A\exp(-E_a/RT)$ (bottom) form of temperature dependence.

where the summation is over the intensities of all the observed ions in each group. The pseudo-first-order rate constants for the deprotonation reactions, k (s^{-1}) and (T) are 796.6 (251 K), 302.1 (254 K), 233.4 (256 K), and 30.7 (265 K), and the corresponding pseudo-second-order rate constants are 7.79×10^{-14}, 2.66×10^{-14}, 1.88×10^{-14}, and 2.32×10^{-15} $cm^3\ s^{-1}$, respectively (10^5-10^6 slower than the collision rate). As observed in Figure 8a, the rate coefficients change rapidly with temperature, and the reaction changes from nearly nonreactive to fast over a range of only 8 K.

The negative temperature dependence of ion−molecule reactions may be expressed in the form $k = CT^{-n}$ that is derived from RRKM considerations, or Arrhenius-type $k = A\exp(-E_a/RT)$; the first form was shown to be linear over a wide temperature range.[46,47] The pseudo-second-order rate coefficients for reaction 2 are plotted in both forms in Figure 8b. The results yield a uniquely large negative temperature coefficient of $k = cT^{-67\pm4}$ (or activation energy of -34 ± 1 kcal mol^{-1}) (higher-order rate coefficients give the same temperature dependence because the experiments were conducted at constant H_2O number density).

The temperature coefficient results from a multibody mechanism in which five or more components need to be assembled in the activated $[C_6H_6^{\bullet+}(H_2O)_4]^*$ complex for the reaction to proceed. In fact, the activation energy is similar to the calculated total binding energy of -35 kcal mol^{-1} of this complex (sum of $\Delta H°_{n-1,n}$, $n = 1-4$ in Table 1). This means that the rates are proportional to the equilibrium concentrations of the reactive $C_6H_6^{\bullet+}(H_2O)_4$ cluster. In other words, only the fraction of the total cluster population that is in the $n \geq 4$ clusters is reactive. Therefore, only this fraction among all the collisions of the clusters with H_2O molecules are reactive, and the small collision efficiency of $10^{-5}-10^{-6}$ reflects this effect. The population of the large reactive clusters increases rapidly with decreasing temperature, and this leads to the large negative temperature coefficient.

The small collision efficiency may be due also in part to an energy barrier to proton transfer. The reaction requires proton transfer in the excited complex from $C_6H_6^{\bullet+}$ to the $(H_2O)_n$ center, apparently over an energy barrier. Every such transfer seems to be dissociative, as nondissociative transfer was ruled out based on the H/D exchange experiments above. In other words, every excited cluster that passes the barrier dissociates to $C_6H_5^{\bullet}$ and $(H_2O)_nH^+$ before stabilizing collisions with the bath gas would convert it to a stable $C_6H_5^{\bullet}(H_2O)_nH^+$ cluster. Although every complex that passes the barrier dissociates, the overall deprotonation reaction proceeds below collision efficiency, and only a fraction of the $[C_6H_6^{\bullet+}(H_2O)_n]^*$ complexes formed by collisions of $[C_6H_6^{\bullet+}(H_2O)_{n-1}]$ with H_2O passes the barrier. Most of the excited $[C_6H_6^{\bullet+}(H_2O)_n]^*$ complexes become stabilized or dissociate back to reactants.

To test this mechanism, we added He as a bath gas to the drift cell. We observed that the deprotonation to form $(H_2O)_nH^+$ is quenched with increasing third-body pressure (the mass spectra are shown in the Supporting Information). This shows that the $[C_6H_6^{\bullet+}(H_2O)_n]^*$ complexes pass the barrier on time scales comparable to about 10^{-7} s collision time with He. Since the complexes that passed the barrier are not stabilized to $C_6H_5^{\bullet}$-$(H_2O)_nH^+$ clusters, these complexes dissociate to products faster than the 10^{-7} collision time.

Scheme 1

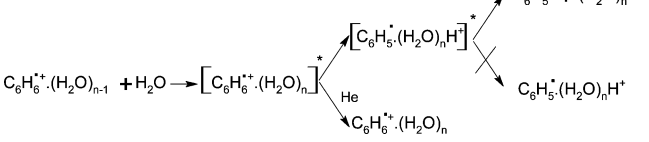

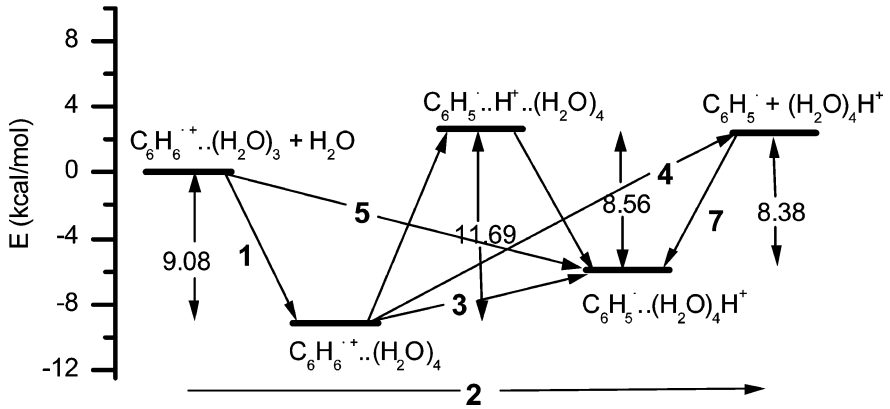

Figure 9. Potential energy surface for the reaction of $C_6H_6^{\bullet+}(H_2O)_3$ with H_2O, yielding $C_6H_6^{\bullet+}(H_2O)_4$ and $C_6H_5^{\bullet} + (H_2O)_4H^+$ products, obtained from ab initio calculations. Energies (kcal/mol) are ZPE-corrected at the MP2//ROHF/6-31+G** level without counterpoise correction. Bold numbers and arrows refer to reactions numbered in the text.

The mechanism can be summarized by Scheme 1.

The mechanism can be understood in reference to the potential energy surface in Figure 9. Some of the excited $[C_6H_6^{\bullet+}(H_2O)_{n-1}]^*$ complexes survive long enough to be stabilized by the bath gas. Other complexes have enough energy to pass the barrier faster. Their internal energies (thermal + excitation) are higher than the barrier and therefore also higher than the $C_6H_5^{\bullet+} + (H_2O)_nH^+$ products whose energy is below the barrier (Figure 9). Therefore, all of the clusters that passed the barrier have enough energy to decompose to the products.

9. Comparison with the Spectroscopic Studies of the $C_6H_6^{\bullet+}(H_2O)_n$ Cluster Cations. The spectroscopic studies of the $(C_6H_6^{\bullet+})(H_2O)_n$ cluster cations suggest that PT reactions occur at $n \geq 4$, resulting in the formation of a phenyl radical solvated by protonated water clusters.[20−26] However, these studies did not observe the well-known electronic spectrum of the phenyl radical ($C_6H_5^{\bullet}$),[26,4747] nor did their dissociation produce the protonated $H^+(H_2O)_n$ water clusters.[22,23] On the other hand, our gas phase studies observe the dissociation products, $H^+(H_2O)_n$, resulting from the stepwise hydration of the benzene cation, but the absence of H/D exchange suggests that the structures of the stepwise hydrated cations are $(C_6H_6^{\bullet+})(H_2O)_n$ and not $(C_6H_5^{\bullet})H^+(H_2O)_n$. Our results also suggest that the PT reaction from $C_6H_6^{\bullet+}$ to the $(H_2O)_n$ center proceeds over an energy barrier, and every such transfer seems to be dissociative to $C_6H_5^{\bullet}$ and $(H_2O)_nH^+$ before stabilizing collisions with the bath gas would convert it to a stable $C_6H_5^{\bullet}(H_2O)_nH^+$ cluster.

The apparent differences in the present stepwise gas phase results and the spectroscopic results of isolated clusters can be resolved by considering the different nature of collisional stabilization in the gas phase system and evaporative stabilization in the isolated cluster system. In the gas phase, the $[C_6H_6^{\bullet+}(H_2O)_n]^*$ complexes pass over the barrier and dissociate into $C_6H_5^{\bullet}$ and $(H_2O)_nH^+$ on time scales faster than the 10^{-7} s collision time needed for stabilization of the $(C_6H_5^{\bullet})H^+(H_2O)_n$ products. In isolated preformed clusters, evaporative stabilization appears to be faster and more efficient than collisional stabilization, and therefore, the PT $(C_6H_5^{\bullet})H^+(H_2O)_n$ products are stabilized by sequential evaporation of water molecules. When n becomes smaller than 4, the $(C_6H_5^{\bullet})H^+(H_2O)_n$ cluster is converted back into $C_6H_6^{\bullet+}(H_2O)_n$. Although all of the dissociation products of the preformed clusters detected by mass spectrometry have the formula $C_6H_6^{\bullet+}(H_2O)_n$, those with $n >$ 4 are actually $(C_6H_5^{\bullet})H^+(H_2O)_n$ and those with $n < 4$ have the hydrated benzene cation structures.

10. Applications in Astrochemistry. Both water and polycyclic aromatics are significant components of interstellar clouds and solar nebulae,[10,14] and benzene itself was also identified recently in protoplanetary nebulae.[10,14,48] These molecules are subject to ionizing radiation, producing stable molecular ions. In these low-temperature environments, water can condense on the ions forming organic-doped ice grains.

The present system models these processes, in particular, because the astrochemical condensation also involves stepwise addition of gas phase molecules. The question of external versus internal solvation and deprotonation is relevant. With internal solvation, the organic component will become isolated in ice. However, external solvation allows the aromatics to remain on the grain surface and undergo reactions with other incoming organic molecules. The calculations on small clusters suggest that such reactive externally solvated structures will be formed when the condensation of water molecules forms ice grains on the aromatic ions. The fact that the charge remains on the aromatic species in the clusters suggests that the aromatic centers can remain reactive for ion−molecule reactions on the grain surfaces. This will also apply to other aromatics that have lower ionization energies. Furthermore, the observed negative temperature coefficients suggest that the low-temperature astrochemical conditions will also allow multibody deprotonation reactions of the ionized aromatics, leaving $C_6H_5^{\bullet}$ radicals that can undergo further interstellar chemistry.

Under the natural conditions, various polar molecules can co-condense on the ionized aromatics, and CO, CO_2, and even H_2 may adsorb and mix with the ices.[10,14] The inclusion of hydrogen bonding polar interstellar molecules that have higher proton affinities than those of H_2O, such as methanol, can further facilitate the deprotonation of the aromatic ions. In further studies, we shall address the properties of such mixed clusters and also clustering on larger ionized interstellar aromatics.

(46) Meot-Ner, M.; Field, F. H. *J. Chem. Phys.* **1974**, *61*, 3742−3749.
(47) Tonokura, K.; Norikane, Y.; Koshi, M.; Nakano, Y.; Nakamichi, S.; Goto, M.; Hashimoto, S.; Kawasaki, M.; Andersen, M. P. S.; Hurley, M. D.; Wallington, T. J. *J. Phys. Chem. A* **2002**, *106*, 5908−5917.
(48) Cernicharo, J.; Heras, A. M.; Tielens, A. G. G. M.; Pardo, J. R.; Herpin, F.; Guelin, M.; Waters, L. B. F. M. *Astrophys. J.* **2001**, *546*, L123−L126.
(49) Keutsch, F. N.; Cruzan, J. D.; Saykally, R. J. *Chem. Rev.* **2003**, *103*, 2533−2578.

V. Conclusions and Outlook

The stepwise binding energies of 1−8 water molecules to benzene$^{\bullet+}$ were determined by equilibrium measurements using an ion mobility cell. The stepwise hydration energies $\Delta H^{\circ}_{n-1,n}$ are nearly constant at 8.5 ± 1 kcal mol^{-1} from $n = 1-6$. Calculations show that in the $n = 1-4$ clusters, the benzene$^{\bullet+}$ ion retains over 90% of the charge, and it is externally solvated, that is, hydrogen bonded to an $(H_2O)_n$ cluster. The binding energies and entropies are larger in the $n = 7$ and 8 clusters, suggesting cyclic or cage-like water structures. The mobilities divide the clusters into two groups of equilibrium-coupled ions, $Bz^{\bullet+}(H_2O)_n$ of $n = 0-2$ and $n = 3-8$. The concentration of the $n = 3$ cluster is always small, suggesting that deprotonation depletes this ion, consistent with the thermochemistry since associative deprotonation $Bz^{\bullet+}(H_2O)_{n-1} + H_2O \rightarrow C_6H_5^{\bullet} + (H_2O)_nH^+$ is thermoneutral or exothermic for $n \geq 4$. Associative intracluster proton transfer $Bz^{\bullet+}(H_2O)_{n-1} + H_2O \rightarrow C_6H_5^{\bullet}\text{-}(H_2O)_nH^+$ would be also exothermic for $n \geq 4$, but lack of H/D exchange with D_2O shows that the proton remains on $C_6H_6^{\bullet+}$ in the observed $Bz^{\bullet+}(H_2O)_n$ clusters. This suggests a barrier to intracluster proton transfer, and as a result, the $[Bz^{\bullet+}(H_2O)_n]^*$ activated complexes either undergo dissociative proton transfer, resulting in deprotonation and generation of $(H_2O)_nH^+$, or become stabilized. The rate constant for the deprotonation reaction shows a uniquely large negative temperature coefficient of $k = cT^{-67\pm4}$ (or activation energy of −34±1 kcal mol^{-1}), caused by a multibody mechanism in which five or more components need to be assembled for the reaction. Future studies will address the hydration and reactions of smaller aromatic cations, such as $C_3H_3^+$, as well as larger cations, such as $C_7H_7^+$, naphthalene$^{\bullet+}$, and anthracene$^{\bullet+}$.

Acknowledgment. This work was funded by National Science Foundation (CHE-0414613) and NASA (NNG04GH45G) Grants to VCU (M.S.E.). S.S. acknowledges support from NIH Grant GM57936.

Supporting Information Available: Figures S1−S3. Three mass spectrum figures showing (1) no H/D exchange upon the injecting of $C_6H_6^{\bullet+}$ into D_2O vapor at 245 K, (2) H/D exchange upon the injection of deuterated 2-fluoropyridine ($C_5H_4FND^+$) into H_2O vapor at 244 K, and (3) the effect of third-body He pressure on quenching the deprotonation reactions to produce $(H_2O)_nH^+$. Complete ref 36. This material is available free of charge via the Internet at http://pubs.acs.org.

JA050477G